

Electronic Supplementary Information (ESI) for the manuscript:

**Ligand Effects on the Dimensionality of Oxamato-Bridged Mixed-Metal Open-Framework
Magnets**

*Jesús Ferrando-Soria, Thais Grancha, Miguel Julve, Joan Cano, Francesc Lloret, Yves
Journaux, Jorge Pasán, Catalina Ruiz-Pérez, and Emilio Pardo*

Experimental Section

Materials. Chloride and nitrate salts of the metals, tetrabutylammonium hydroxide, ethyl chlorooxoacetate and 2,6-dialkylaniline derivatives were purchased from commercial sources and used as received. The ligands and the mononuclear copper(II) complexes were prepared as previously reported.⁹

Preparation of $(n\text{-Bu}_4\text{N})_2[\text{Cu}(\text{Me}_2\text{pma})_2] \cdot 2\text{H}_2\text{O}$ and $(n\text{-Bu}_4\text{N})_2[\text{Cu}(\text{Et}_2\text{pma})_2] \cdot 2\text{H}_2\text{O}$: The tetrabutylammonium salts of the copper(II)-L (L = Me₂pma and Et₂pma) precursors were prepared by following a synthetic procedure reported previously⁹ which consists of reacting the respective proligands HEtL (Me₂pma and Et₂pma) with CuCl₂ · 2H₂O (0.17 g, 1 mmol) in water using a 1.0 M methanol solution of (n-Bu₄N)OH (4 mL, 4 mmol) as a base. They were isolated as their dihydrated tetrabutylammonium salts. **(n-Bu₄N)₂[\text{Cu}(\text{Me}_2\text{pma})_2] · 2\text{H}_2\text{O}**: Yield: 89%; Elemental analysis calcd. (%) for C₅₂H₉₄CuN₄O₈ (965): C 64.63, H 9.73, N 5.80; found: C 64.52, H 9.67, N 5.73; IR (KBr): ν = 3421 (O–H), 1649, 1620 cm⁻¹ (C=O); **(n-Bu₄N)₂[\text{Cu}(\text{Et}_2\text{pma})_2] · 2\text{H}_2\text{O}**: Yield: 82%; Elemental analysis calcd. (%) for C₆₀H₁₁₀CuN₄O₈ (1078): C 66.78, H 10.27, N 5.19; found: C 66.21, H 10.00, N 5.19; IR (KBr): ν = 3432(O–H), 1633, 1610 cm⁻¹ (C=O).

Preparation of $(n\text{-Bu}_4\text{N})_4[\text{Mn}_4\text{Cu}_6(\text{Me}_2\text{pma})_{12}(\text{DMSO})_2] \cdot 8\text{DMSO} \cdot 2\text{H}_2\text{O}$ (1**) and $(n\text{-Bu}_4\text{N})_4[\text{Mn}_4\text{Cu}_6(\text{Et}_2\text{pma})_{12}] \cdot \text{DMSO} \cdot 10\text{H}_2\text{O}$ (**2**):** Well-formed pale green tiny prisms of **1** and **2**, which were suitable for synchrotron diffraction, were obtained by following a synthetic procedure already reported.⁹ In a typical experiment, Mn(NO₃)₂ · 4H₂O (0.025 g, 0.1 mmol) was dissolved in hot DMSO (25 mL) and added dropwise to solutions of (n-Bu₄N)₂[\text{Cu}(\text{Me}_2\text{pma})_2] · 2H₂O (0.482 g, 0.5 mmol) and (n-Bu₄N)₂[\text{Cu}(\text{Et}_2\text{pma})_2] · 2H₂O (0.511 g, 0.5 mmol) respectively, dissolved in hot DMSO (25 mL) at 80 °C. The resulting dark-green solutions were filtered while hot and the filtrates were allowed to stand at RT. After several days, green crystals of **1** and **2** appeared, and they were filtered off and air-dried. Yield: 39% (**1**) and 44% (**2**); **1**: Elemental analysis calcd. (%) for C₂₀₄H₃₁₆Cu₆Mn₄N₁₆O₄₈S₁₀ (4682.5): C 52.33, H 6.80, N 4.78, S 6.85; found: C 52.19, H 6.62, N 4.79, S 6.81; IR (KBr): ν = 3432 (O–H), 1601, 1581 cm⁻¹ (C=O). **2**: Elemental analysis calcd. (%) for C₂₁₀H₃₂₆Cu₆Mn₄N₁₆O₄₇S (4460.0): C 56.55, H 7.37, N 5.02, S 0.72; found: C 56.62, H 6.67, N 5.12, S 0.69; IR (KBr): ν = 3448 (O–H), 1626, 1601, 1580 cm⁻¹ (C=O).

Physical Techniques. Elemental analyses (C, H, N) were performed at the Microanalytical Service of the Universitat de València (Spain). IR spectra were recorded on a Perkin–Elmer 882 spectrophotometer as KBr pellets.

Crystal Structure Data Collection and Refinement. Crystal data for **1**: C₄₀₇H₆₂₇Mn₈Cu₁₂N₃₂O₉₅S₂₀, M_r = 9331.89, triclinic, space group *P*-1, *a* = 16.861(3), *b* = 18.896(4), *c* = 42.547(9) Å, α = 88.032(9), β = 88.979(10), γ = 66.792(9) $^\circ$, *V* = 12451(4) Å³, *T* = 100(2) K, λ = 0.73850 Å, *Z* = 1, ρ_{calc} = 1.244 g cm⁻³, μ = 0.939 mm⁻¹, 42164 unique reflections [170884 measured (*R*_{int} = 0.1074)] and 31025 observed with *I* > 2 σ (*I*), 1.30 $^\circ$ $\leq \theta \leq$ 25.81 $^\circ$, *R* = 0.1609 (0.1862 for all data), *wR* = 0.4597 (0.4801 for all data) with 2510 parameters and 37 restraints, the final Fourier-difference map showed maximum and minimum height peaks of 3.251 and -1.730 e Å⁻³. Crystal data for **2**: C₂₁₀H_{324.698}Mn₄Cu₆N₁₆O_{46.349}S, M_r = 4448.27, monoclinic, space group *C*2/c, *a* = 24.393(5), *b* = 23.706(5), *c* = 24.523(3) Å, β = 112.81(3) $^\circ$, *V* = 13072(5) Å³, *T* = 100(2) K, λ = 0.7385 Å, *Z* = 2, ρ_{calc} = 1.126 g cm⁻³, μ = 0.815 mm⁻¹, 11486 unique reflections [87432 measured (*R*_{int} = 0.0747)] and 7446 observed with *I* > 2 σ (*I*), 1.25 $^\circ$ $\leq \theta \leq$ 26.12 $^\circ$, *R* = 0.1556 (0.1884 for all data), *wR* = 0.4515 (0.4747 for all data) with 494 parameters and 37 restraints, the final Fourier-difference map showed maximum and minimum height peaks of 1.222 and -0.715 e Å⁻³. The collected data for both compounds were indexed, integrated and scaled with the HKL2000 program.¹ All the measured independent reflections were used in the analysis. The structure was solved by direct methods and refined with full-matrix least-squares technique on *F*² using the SHELXS-97 and SHELXL-97 programs.² All non-hydrogen atoms of **1** were refined with anisotropic thermal parameters except the oxygen atoms of the two crystallization water molecules and the crystallization dimethylsulfoxide molecules. The hydrogen atoms were set on calculated positions and refined with a riding model. Geometrical and displacement parameters restraints were applied on dimethylsulfoxide molecules and disordered diethylphenyloxamate and tetrabutylammonium ligands. In the case of **2**, all non-hydrogen atoms were refined with anisotropic thermal parameters except those of the carbon atoms of the disordered diethyl-phenyl groups of the diethylphenyloxamate ligands and the solvent molecules (water, dimethyl sulfoxide and tetrabutylammonium molecules) and the hydrogen atoms were set on calculated positions. A diethylphenyloxamate ligand is disordered between two positions around Cu(3) and a residual electron density found near one of these ligands was assigned to a partially occupied water molecule. Crystallographic data (excluding structure factors) for the structure reported in this paper have been deposited with the Cambridge Crystallographic Data Centre as supplementary publication no. CCDC-852495 (**1**) and CCDC-852496 (**2**). Copies of the data can be obtained free of charge on application to CCDC, 12 Union Road, Cambridge CB21EZ, UK (fax: (+44) 1223-336-033; e-mail: deposit@ccdc.cam.ac.uk).

¹ Z. Otwinowski, W. Minor, *Processing of X-ray Diffraction Data Collected in Oscillation Mode*, Methods in Enzymology 276, Macromolecular Crystallography, part A, **1997**, 307, C. W. Carter, Jr., R. M. Sweet, Eds., Academic Pres (New York).

² Sheldrick, G. M. *SHELX97*, release 97-2; Institut für Anorganische Chemie der Universität Göttingen: Göttingen, Germany, **1998**.

Magnetic Measurements. Variable-temperature (2.0–300 K) magnetic susceptibility under an applied field of 1 T ($T \geq 50$ K) and 100 G ($T < 50$ K) and variable-field (0–5.0 T) magnetization measurements at $T = 2.0$ K were carried out on polycrystalline samples of **1** and **2** with a Quantum Design MPMS SQUID-based magnetometer. The magnetic susceptibility data were corrected for the diamagnetism of the constituent atoms and the sample holder.

Magnetic Properties.

The magnetic properties of **1** and **2**, in the form of the $\chi_M T$ versus T plot (χ_M being the molar magnetic susceptibility per Cu_3Mn_2 unit and T the temperature) are represented in Fig. S6a. At room temperature, $\chi_M T$ is equal to 8.04 and $8.15 \text{ cm}^3 \text{ mol}^{-1} \text{ K}$ for **1** and **2**, respectively. These values are well below that expected for the sum of three square-planar Cu^{II} ions ($\chi_M T = 0.40 \text{ cm}^3 \text{ mol}^{-1} \text{ K}$ with $S_{\text{Cu}}=1/2$ and $g_{\text{Cu}} = 2.1$) and two octahedral high-spin Mn^{II} ions ($\chi_M T = 4.37 \text{ cm}^3 \text{ mol}^{-1} \text{ K}$ with $S_{\text{Mn}}= 5/2$ and $g_{\text{Mn}} = 2.0$), suggesting the occurrence of a moderate *intramolecular* antiferromagnetic interaction between the Cu^{II} and Mn^{II} ions through the oxamate bridges. Upon cooling, $\chi_M T$ slowly decreases and attains minima at *ca.* 132 and 136 K for **1** and **2** respectively, supporting the ferrimagnetic behaviour. Further cooling shows an abrupt increase of $\chi_M T$ at 15 and 25 K for **1** and **2** respectively, to reach maximum values of 1448 (**1**) and 3325 (**2**) $\text{cm}^3 \text{ mol}^{-1} \text{ K}$ at *ca.* 10 and 16 K.

The values of the saturation magnetization (per $\text{Cu}^{\text{II}}_3\text{Mn}^{\text{II}}_2$ unit) of 6.72 (**1**) and 6.80 (**2**) $N\beta$, at 2.0 K are consistent with that predicted for an antiparallel alignment of the spins of three Cu^{II} and two Mn^{II} ions [$M_s = (2g_{\text{Mn}}S_{\text{Mn}}-3g_{\text{Cu}}S_{\text{Cu}}) = 6.85 N\beta$ with $g_{\text{Mn}} = 2.00$ and $g_{\text{Cu}} = 2.10$]. Moreover, the magnetization isotherms at 2.0 K show extremely fast saturation for both compounds with about 98 % of the maximum magnetisation value being reached under a dc field of *ca.* 500 (**1**) and 1000 G (**2**). This reveals very strong short-range correlation along the 2D (**1**) and 3D (**2**) framework favouring the antiparallel alignment of the spins of Cu^{II} and Mn^{II} ions (Figure S6b).

Quantum Monte Carlo Calculations. Quantum Monte Carlo (QMC) simulations were carried out on the CuMn oxamate 2D (**1**) and 3D (**2**) networks with the topologies shown in Scheme 1 (see text). The decoupled cell method described elsewhere,^{3,4} where the probability of a spin flip is calculated from the exact solution of a model that is made up of this spin and the first and second neighbours was used. The network models were built from cells with 18 (**1**) and 20 (**2**) sites that were repeated 10x10 and 2x5x10

³ Homma, S., Matsuda, H. & Ogita, N. Decoupled cell method Monte Carlo simulation for quantum spin systems. *Prog. Theor. Phys.* **75**, 1058–1065 (1986).

⁴ Toma, L. *et al.* Nuclearity controlled cyanide-bridged bimetallic $\text{Cr}^{\text{III}}-\text{Mn}^{\text{II}}$ compounds: synthesis, crystal structures, magnetic properties and theoretical calculations. *Chem. Eur. J.* **10**, 6130–6145 (2004).

times, respectively. Moreover, periodic boundary conditions were imposed. To avoid a freezing of spin configuration, we have used a low cooling rate according to the following equation:

$$T_{i+1} = 0.98 * T_i$$

The number of Monte Carlo steps per site at each temperature was fifty thousand, and a ten per cent was used in the thermalization process. Finally, the $\chi_M T$ product was evaluated from the magnetization fluctuation. From the results obtained by following this strategy, we have procured empirical laws which allow the simulation of the empirical data and that relate the $\chi_M T$ product with the reduced temperature, $T_r = T/J$, where J is expressed in K. These laws were derived by minimizing a quotient between two polynomials that becomes as:

$$XT = \frac{5}{4} g_{Mn}^2 \frac{\sum_{i=0}^5 B_i (1 + A_i \alpha^2) T_r^i}{\sum_{i=0}^5 C_i (1 + D_i \alpha^2) T_r^i} \quad (S1)$$

with $\alpha = g_A/g_B$, and where A and B are the spins of Mn^{II} ($S = 5/2$) and Cu^{II} ($S = 1/2$). The corresponding coefficients for **1** and **2** are listed in Tables S1 and S2, respectively. This empirical law is only valid for $0.9 \leq \alpha \leq 1.2$ and $T_r \geq 0.4$.

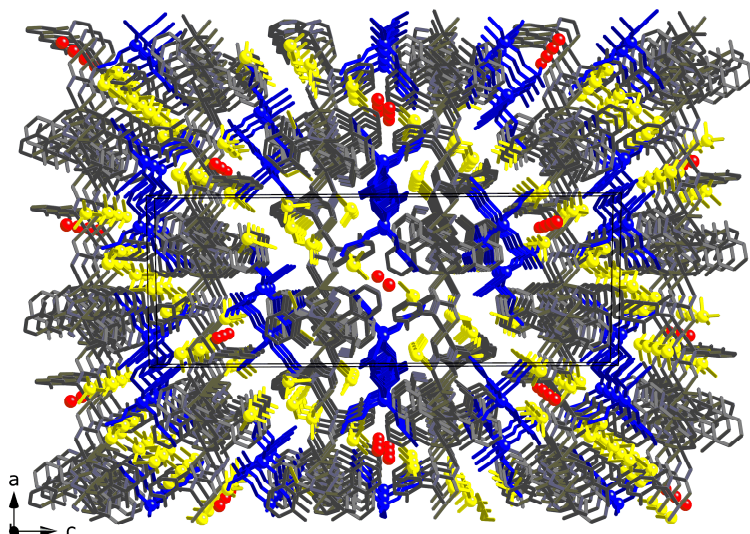


Fig. S1 Crystal packing view of **1** along the *b* axis showing the filling of the interlayer spaces by *n*-Bu₄N⁺ counterions (blue) as well as H₂O (red) and DMSO (yellow) molecules.

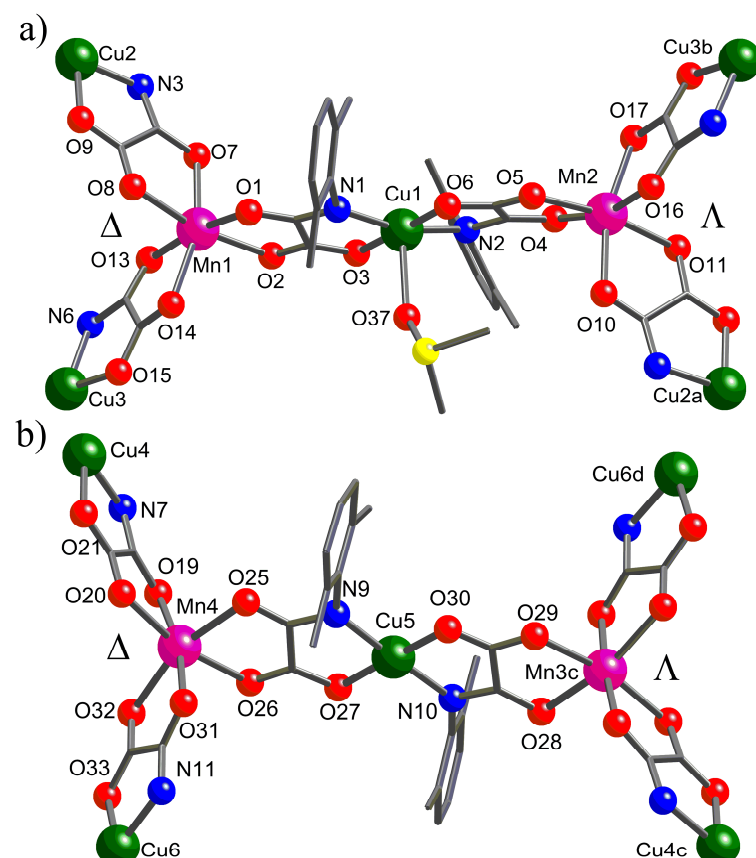


Fig. S2 (a) and (b) Perspective views of two fragments of **1** with the atom labelling of the metal coordination environments. [Symmetry codes: (a) = $x, y - 1, z$; (b) = $x + 1, y - 1, z$; (c) = $x, y + 1, z$; (d) = $x + 1, y, z$].

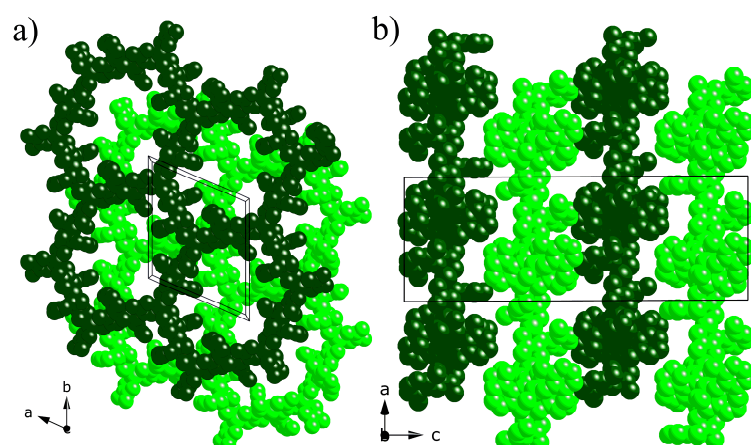


Fig. S3 Perspective views of the packing of the adjacent layers of **1** along the *c* (a) and *b* (b) axis, respectively. The two different A and B planes are colored in dark and pale green. The counterions and the solvent molecules have been omitted for clarity.

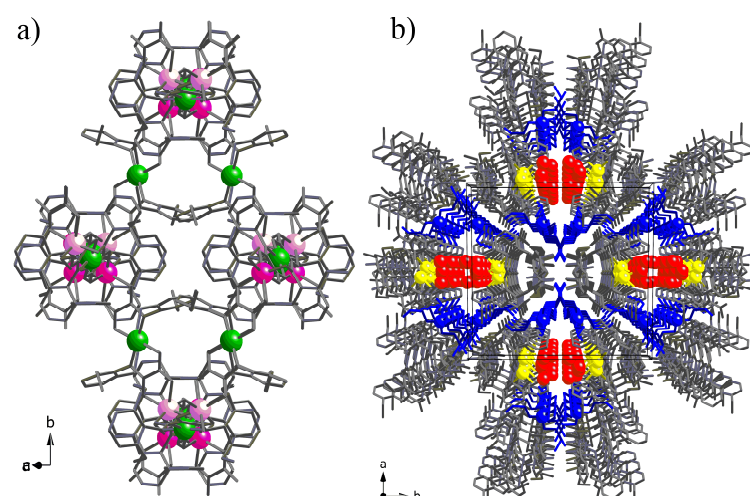


Fig. S4 (a) Perspective view of the 2D anionic network of **2** along the [10-1] direction. Metal and ligand atoms are represented by balls and sticks, respectively (Cu, green; A -Mn, purple; $(\text{A})\text{-Mn}$, pink). (b) View of the crystal packing of **2** along the *c* axis showing the filling of the medium pores of the open-framework structure by the *n*-Bu₄N⁺ counterions (blue) as well as the free water (red) and DMSO (yellow) molecules.

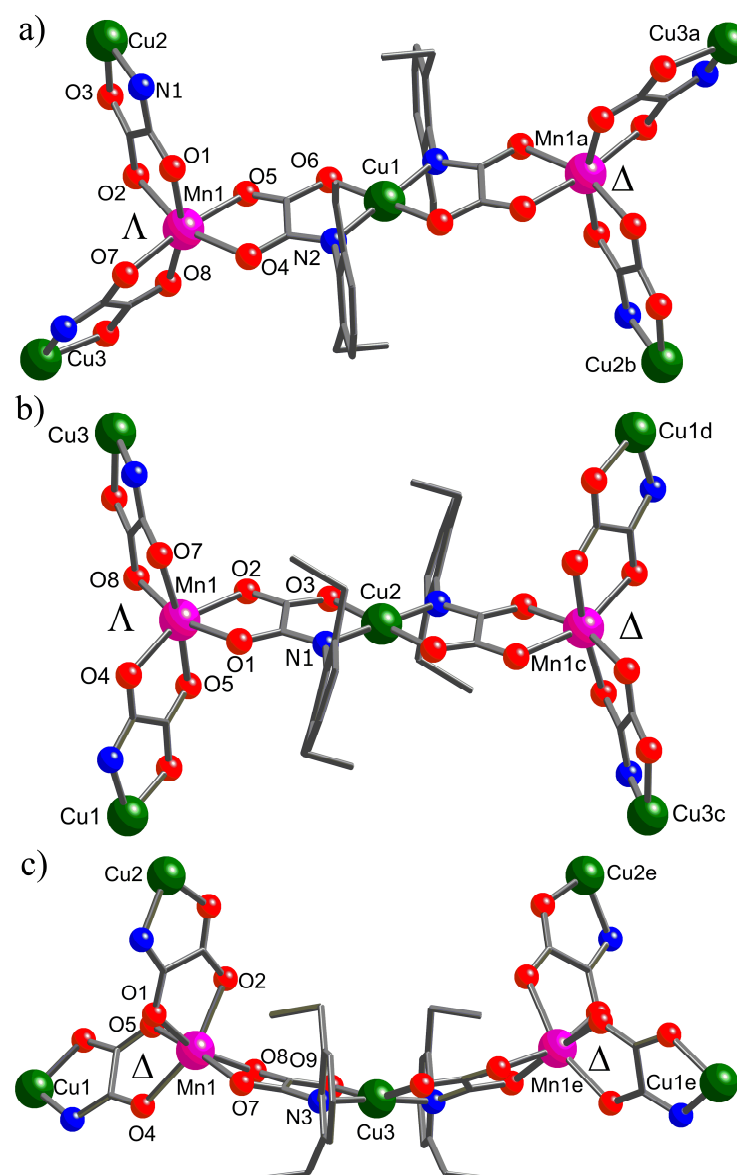


Fig. S5 (a), (b), and (c) Perspective views of three fragments of **2** with the atom labelling of the metal coordination environments. [Symmetry codes: (a) = $-x + 1/2, -y + 1/2, -z + 1$; (b) = $x - 1/2, y - 1/2, z$; (c) = $-x + 1, -y + 1, -z + 1$; (d) = $x + 1/2, y + 1/2, z$; (e) = $-x + 1, y, -z + 1/2$].

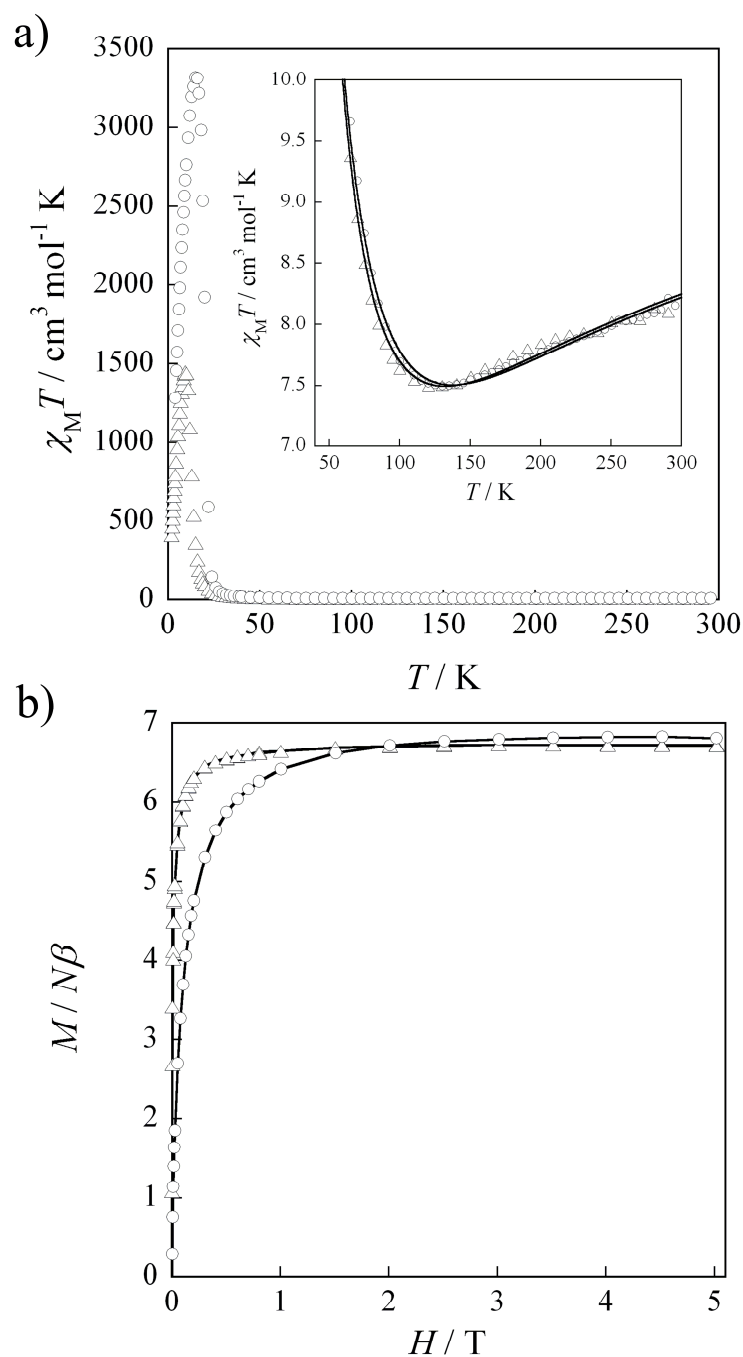


Fig. S6 (a) Temperature dependence of $\chi_M T$ for **1** (Δ) and **2** (\circ). The inset shows a detail of the minima of $\chi_M T$. The solid lines correspond to the Quantum Monte Carlo simulations (see text). (b) Field dependence of M for **1** (Δ) and **2** (\circ) at 2.0 K.

Table S1 Values of the polynomial coefficients in the empirical law used to reproduce the temperature dependence of the magnetic susceptibility, the strength of the magnetic coupling and the g-factor of a regular “expanded honeycomb” 2D network (1) (eq. S1).^[a,b]

i	A _i	B _i	C _i	D _i
0	0.224554	-8.363909	-16.27368	0.132579
1	3.700845	3.905049	10.70158	1.590336
2	-1.512782	32.90925	5.923013	-8.524822
3	2.463738	35.40932	-11.08573	-5.304042
4	-1.327145	65.05818	-0.446410	38.95068
5	3.297255	11.29174	1.809345	8.736334

^[a] Eq. S1 is only valid for $0.9 \leq \alpha \leq 1.2$ and $T_r \geq 0.4$. ^[b] J is given in K in eq. S1.

Table S2 Values of the polynomial coefficients in the empirical law used to reproduce the temperature dependence of the magnetic susceptibility, the strength of the magnetic coupling and the *g*-factor of a regular “multidirectional brickwall” 3D network (**2**) (eq. S1).^[a,b]

i	A _i	B _i	C _i	D _i
0	2.166836	-94.980823	-63.79801	0.084642
1	-0.603182	-459.3626	93.75025	-0.785419
2	-157.4099	-7.019887	-62.71180	-3.004059
3	187.3421	-12.24247	1.37200	-195.8532
4	-2.586003	-723.3612	-2.34414	-138.5241
5	-7.326241	95.87427	-62.37040	4.997786

^[a] Eq. S1 is only valid for $0.9 \leq \alpha \leq 1.2$ and $T_r \geq 0.4$. ^[b] *J* is given in K in eq. S1.